Journal of Magnetism and Magnetic Materials 471 (2019) 381–387

Contents lists available at ScienceDirect

Journal of Magnetism and Magnetic Materials

journal homepage: www.elsevier.com/locate/jmmm

Research articles

Combined antitumor effect of surface-modified superparamagnetic maghemite nanoparticles and a vitamin E derivative on experimental Walker-256 mammary gland carcinosarcoma

Beata A. Zasońska[a], Vitaliy Igorovych Pustovyy[b], Andriy Valeriyovich Babinskiy[b], Olga Mikhailovna Palyvoda[b], Vasyl Fedorovich Chekhun[c], Igor Todor[c], Eduard Petrovský[d], Oleksandr Ivanovich Kuzmenko[b], Daniel Horák[a,*]

[a] Institute of Macromolecular Chemistry, Academy of Sciences of the Czech Republic, Heyrovského nám. 2, 162 06 Prague 6, Czech Republic
[b] Palladin Institute of Biochemistry, NASU, 9 Leontovich St., 01601 Kiev, Ukraine
[c] R. E. Kavetsky Institute of Experimental Pathology, Oncology and Radiobiology, NASU, 45 Vasylkivska St., 03022 Kiev, Ukraine
[d] Institute of Geophysics, Academy of Sciences of the Czech Republic, Boční II/1401, 141 31 Prague 4, Czech Republic

ARTICLE INFO

Keywords:
Superparamagnetic
Nanoparticles
α-Tocopherol
Mammary gland carcinosarcoma

ABSTRACT

In a search for efficient anti-tumor agent, silica-coated superparamagnetic nanoparticles were designed and used in combination with vitamin E derivative as a potential new tool for anticancer treatment. The particles were characterized by numerous techniques, such as transmission electron microscopy and dynamic light scattering to determine the particle morphology and size both in dry state and water, atomic absorption spectroscopy to analyze the iron content, Fourier-transform infrared spectroscopy to confirm the presence of the functional groups, and vibrating sample magnetometry to determine the magnetic properties and content of maghemite. The next aim was to assess effect of the nanoparticles on suppression of experimental mammary gland carcinosarcoma W-256. Strong antitumor effect was achieved only with combined application of γ-Fe_2O_3@SiO_2 and acetate derivative of α-tocopherol (Toc-6-Ac) resulting in 58% of tumor volume reduction. The results were compared with those obtained with poly(*N,N*-dimethylacrylamide)-coated iron oxide particles described earlier.

1. Introduction

Magnetic iron oxide nanoparticles have recently received a great deal of attention due to their potential biomedical applications [1–4] as contrast agents in magnetic resonance imaging (MRI) [5], magnetic separation of cells and proteins [1], drug delivery [6,7], hyperthermia [8,9], etc. Iron oxide nanoparticles carrying anticancer drugs, such as flutamide [10] or doxorubicin, demonstrated antiproliferative effect on breast and prostate cancer cell lines [11]. Various procedures have been suggested for synthesis of iron oxide nanoparticles involving co-precipitation of Fe(II) and Fe(III) salts, hydrothermal, sol-gel and solvothermal reactions [12], sonolysis [13], flow injection, electrochemical and aerosol/vapor methods, thermal decomposition of organo-metallic compounds, microbial [14] and laser evaporation syntheses, microemulsion [15], etc. Aim of these syntheses was to form stable aqueous iron oxide colloids with high saturation magnetization. At the same time, the particles should be preferably uniform in size to confer them the same physical, chemical, and biological properties [16,17].

A plethora of surface modifications was suggested to prevent particle aggregation and to introduce functionalities for attachment of a target biomolecule [18–20]. Uncoated magnetic particles might have some limitations in practical applications as they tend to coagulate or undergo rapid biodegradation during exposition to biological media. There is considerable interest in introducing specificity, e.g., anticancer effect, by functionalizing the nanoparticles with polymers, antibodies, drugs or ligands directed against cancer [21]. Current literature suggests that vitamin E may be a suitable candidate for the adjuvant treatment of cancer [22–28]. Vitamin E is a well-known antioxidant that acts as an essential component of biological membranes and circulating lipoproteins. Vitamin E analogues epitomized by *α*-tocopheryl succinate represent an exciting group of novel anticancer agents of potentially high pharmacological importance [29]. *α*-Tocopheryl succinate inhibits the growth of breast cancer cells *in vitro* and *in vivo* [27,30]. The mechanism of its *in vivo* effects may involve inhibition of tumor angiogenesis and VEGF gene expression [31]. Vitamin E

* Corresponding author.
E-mail address: horak@imc.cas.cz (D. Horák).

https://doi.org/10.1016/j.jmmm.2018.10.006
Received 23 April 2018; Received in revised form 5 September 2018; Accepted 1 October 2018
Available online 03 October 2018
0304-8853/

analogues with anticancer activity are typically hydrophobic esters which are completely hydrolyzed upon intestinal uptake [32,33].

In this report, functionalizable silica, which is well-known for its biocompatibility and easy bioconjugation with various drugs [34], was used as a suitable inert coating to prevent leakage of iron ions and to reduce Fe oxidation-reduction reactions in the living organism. Minimized redox reactions of the magnetic particles are believed to affect antitumor activity [35–37]. In contrast, increased redox activity of combined administration of γ-Fe_2O_3 and acetate derivative of α-tocopherol with six-carbon side chain (Toc-6-Ac) is expected to restore the antitumor activity. Although several methods have been suggested for preparation of composite magnetic silica nanoparticles [38,39], the most popular synthesis is based on the sol-gel process developed by Stöber [40]. The method produces silica by *in situ* hydrolysis and condensation of a sol-gel precursor and is especially suitable for coating of the magnetic nanoparticles dispersed in polar solvents such as water or ethanol. Silica-modified maghemite (γ-Fe_2O_3) nanoparticles were thus prepared and tested in combination with Toc-6-Ac for treatment of mammary gland carcinosarcoma in an animal model. The results were compared with those achieved by previously described maghemite nanoparticles coated with poly(*N,N*-dimethylacrylamide) (γ-Fe_2O_3@PDMA) [41].

2. Experimental

2.1. Materials

$FeCl_2{\cdot}4H_2O$, $FeCl_3{\cdot}6H_2O$, and tetramethyl orthosilicate (TMOS) were purchased from Sigma-Aldrich (Steinheim, Germany). Sodium hypochlorite solution (5 wt%) was from Bochemie (Bohumín, Czech Republic), ammonium hydroxide solution (25%), methanol, and ethanol were from Lach-Ner (Neratovice, Czech Republic). Doxorubicin was obtained from Arterium (Kiev, Ukraine). α-Tocopherol acetate with a six-carbon side chain (Toc-6-Ac) was prepared according to a patent [42]. Poly(*N,N*-dimethylacrylamide)-coated maghemite (γ-Fe_2O_3@PDMA) nanoparticles were prepared earlier [41]. Ultrapure Q-water ultrafiltered on a Milli-Q Gradient A10 system (Millipore, Molsheim, France) was used for preparation and washing solutions.

2.2. Preparation of maghemite (γ-Fe_2O_3) nanoparticles

Iron oxide nanoparticles were prepared from iron(III) and iron(II) chloride according to a previously described standard procedure [43]. Shortly, aqueous 0.2 M $FeCl_3$ solution (100 ml), aqueous 0.2 M $FeCl_2$ solution (50 ml), and aqueous 0.5 M NH_4OH (100 ml) were sonicated with 120 W power (Sonicator W-385; Heat Systems-Ultrasonics; Farmingdale, NY, USA) for 5 min. The mixture was added to 3.3 wt% NH_4OH solution (460 ml) and stirred (200 rpm) at 23 °C for 1 h. Resulting magnetite was magnetically separated and washed by Q-water until peptization and the colloid was sonicated with 5 wt% sodium hypochlorite solution (16 ml) for 5 min. The precipitate was magnetically separated and repeatedly washed with Q-water under formation of γ-Fe_2O_3 colloid.

2.3. Preparation of silica-modified γ-Fe_2O_3 nanoparticles (γ-Fe_2O_3@SiO_2)

Silica-coated iron oxide nanoparticles were synthesized by modification of Stöber's method [40,44]. Briefly, 25% NH_4OH (3 ml) was added to aqueous γ-Fe_2O_3 (100 mg) colloid (10 ml) and the mixture was sonicated for 5 min. Ethanol (60 ml) and TMOS (4 ml) were added and the mixture was stirred at 50 °C for 18 h. The resulting γ-Fe_2O_3@SiO_2 nanoparticles were carefully washed by magnetic separation and centrifugation using methanol, ethanol, and several portions of Q-water to remove reaction by-products.

2.4. Characterization of nanoparticles

γ-Fe_2O_3 and γ-Fe_2O_3@SiO_2 nanoparticles were characterized by a Tecnai Spirit G2 transmission electron microscope (TEM; FEI; Brno, Czech Republic). The number-average diameter (D_n) and polydispersity index (PDI = D_w/D_n) were calculated from ~300 particles using Atlas program. The hydrodynamic particle size (D_h) of γ-Fe_2O_3 and γ-Fe_2O_3@SiO_2 particles was determined by dynamic light scattering (DLS) using a Nano-ZS Model ZEN3600 Zetasizer (Malvern Instruments; Malvern, UK) at pH 7. Iron content was determined with a Perkin-Elmer 3110 (Norwalk, CT, USA) atomic absorption spectrometer (AAS) using a solution obtained by mineralization of a sample with dilute HCl (1:1) at 80 °C for 1 h. Fourier-transform infrared (FTIR) spectra were recorded in an attenuated total reflection (ATR) mode using a Thermo Nicolet Nexus 870 FTIR spectrometer (Madison, WI, USA). The magnetization was measured using an EV9 vibrating sample magnetometer (VSM; DSM Magnetics, ADE Corporation; Lowell, MA, USA) at a room temperature (RT).

2.5. Biological experiments

2.5.1. Blood serum preparation, white and red blood cells counts, bilirubin content, and blood enzyme activities

After the euthanasia, blood was taken from Wistar rats (200 g body weight) by heart puncture with a syringe, kept at 25 °C for 0.5 h, and centrifuged for 15 min at 1500 *g* to obtain serum, which was stored at −80 °C.

The numbers of white and red blood cells were calculated in blood (5 ml) placed in a Li-heparin blood collection tube (Vacutest Kima; Arzergande, Italy), which was turned upside down two times, using a PCE210 apparatus (Erma; Tokyo, Japan).

The level of bilirubin and activities of alanine aminotransferase (ALT) and aspartate aminotransferase (AST) in blood plasma were determined using a Bio- and immunochemistry analyzer 2990 (Global Biomarketing Group; Kiev, Ukraine) [45–47].

2.5.2. Determination of antitumor activity

As a mammary gland tumor model for *in vivo* experiments, Walker-256 carcinosarcoma (W-256, female Wistar rats, 200 g body weight) was used. To introduce the tumor cells, suspension of tumor tissue (23% W-256) in cell culture medium 199 (0.4 ml) was injected under the skin of the animal back. Then, the rats were divided into seven groups: (i) tumor-bearing controls without treatment (except saline), (ii) animals with tumor size 7–10 mm treated with doxorubicin (1.5 mg/kg) usually on the third day from W-256 transplantation, (iii) tumor-bearing animals treated with Toc-6-Ac, (iv) γ-Fe_2O_3, (v) γ-Fe_2O_3@SiO_2, (vi) γ-Fe_2O_3 and Toc-6-Ac, and (vii) γ-Fe_2O_3@SiO_2 and Toc-6-Ac. In (ii), the doxorubicin was administered intraperitoneally, while the agents (typically 25 mg Toc-6-Ac and 10 mg nanoparticles per kg) were administered *per os* into the stomach in other groups. The groups had 10 animals, which received five injections of doxorubicin, γ-Fe_2O_3, or γ-Fe_2O_3@SiO_2 nanoparticles, or ten injections of Toc-6-Ac daily within 10 days. After completion of the experiment, size of the tumor was evaluated by a caliper and the tumor volume (V; cm^3) calculated according to the formula [48]:

$$V = (4/3) \times \pi \times (L/2) \times (W/2) \times (D/2)/1000\ ,$$

where L stands for length, W – width, and D – depth (mm) of tumor.

2.5.3. Ethical issues of animals use

Experiments with non-transgenic Wistar female rats followed the EC regulations and were approved by the ethical committee of the Palladin Institute of Biochemistry and the R.E. Kavetsky Institute of Experimental Pathology, Oncology and Radiobiology. The animals were kept in a special facility and euthanasia was performed by necropsy after carbon dioxide asphyxiation [49,50].

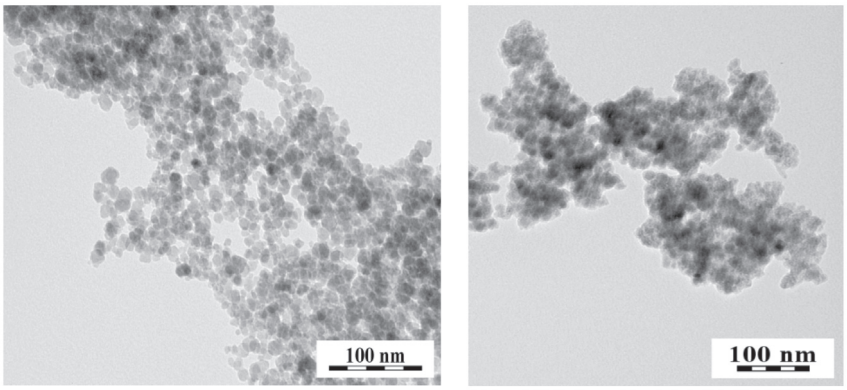

Fig. 1. TEM micrographs of (a) γ-Fe_2O_3 and (b) γ-Fe_2O_3@SiO_2 nanoparticles.

2.5.4. Data analysis

To compare experimental differences, two-tailed Student's *t*-test with the significance level $P < 0.05$ was used. All data were presented as means ± standard error (SE).

3. Results and discussion

3.1. γ-Fe_2O_3@SiO_2 nanoparticles, their morphology and composition

Starting maghemite (γ-Fe_2O_3) nanoparticles were prepared by alkaline co-precipitation of ferrous and ferric ions followed by oxidation with sodium hypochlorite. Silica-coated nanoparticles were then produced by simple hydrolysis and condensation of TMOS in the presence of γ-Fe_2O_3 nanoparticles. TEM micrographs showed that the number-average diameter D_n of γ-Fe_2O_3 was 11 nm with polydispersity index PDI = 1.13 (Fig. 1 a) documenting a relatively narrow particle size distribution. Size of the γ-Fe_2O_3@SiO_2 particles can be controlled by changing the TMOS/γ-Fe_2O_3 ratio and polymerization conditions, such as temperature, pH, or hydrodynamic parameters (type of the reactor, stirring speed, etc.) [51]. In this study, TMOS hydrolysis and condensation was catalyzed by ammonium hydroxide base to transform silanols to siloxane bonds. Size of the γ-Fe_2O_3@SiO_2 nanoparticles increased to D_n = 16 nm (PDI = 1.09), which suggests that the shell thickness reached ~2.5 nm (Fig. 1b). Tiny iron oxide particles tended to form aggregates during drying (Fig. 1), nevertheless they formed a colloidally stable dispersion in water. Compared to TEM, hydrodynamic diameter of both γ-Fe_2O_3 and γ-Fe_2O_3@SiO_2 particles in water was larger, amounting to 180 and 244 nm, respectively (Table 1). Larger D_h of γ-Fe_2O_3@SiO_2 than that of γ-Fe_2O_3 was due to the presence of silica shell around the iron oxide particles. It should be also noted that the hydrodynamic diameter D_h of particles determined by DLS in water was always larger than the number-average diameter D_n of dry particles according to TEM. Moreover, D_h represents z-average, which is an intensity-based value highly sensitive to the presence of a small number of aggregates and should not be confused with number-mean value.

To further confirm coating of the γ-Fe_2O_3 particles with silica, AAS and ATR FTIR spectroscopy was used. While the starting γ-Fe_2O_3 nanoparticles contained 67.4 wt% of Fe according to AAS, amount of iron in the γ-Fe_2O_3@SiO_2 decreased to 41.5 wt% due to the presence of the silica shell (Table 1). In the FTIR spectrum of the γ-Fe_2O_3 particles, strong absorption bands at ~540 and 618 cm^{-1} were ascribed to Fe-O bonds (Fig. 2). After modification of the γ-Fe_2O_3 with silica, the presence of SiO_2 shell was confirmed by a peak at ~556 cm^{-1} ascribed to Fe-O-Si bonds and by bands at 1058 and 958 cm^{-1} assigned to SiO-H and Si-O-Si groups, respectively.

Table 1
Characterization of the nanoparticles.

Particles	D_n[a] (nm)	PDI[b]	D_h[c] (nm)	Fe[d] (wt%)	M_s[e] (A·m^2/kg)
γ-Fe_2O_3	11	1.13	180	67.4	56.5
γ-Fe_2O_3@SiO_2	16	1.09	244	41.5	51

[a] Number-average particle diameter (TEM).
[b] Polydispersity index (TEM).
[c] Hydrodynamic diameter (DLS).
[d] From atomic absorption spectroscopy.
[e] Saturation magnetization (VSM).

3.2. Magnetic measurements

Another characterization of the γ-Fe_2O_3 and γ-Fe_2O_3@SiO_2 nanoparticles involved analysis of magnetic hysteresis curves, which showed the dependence of the induced magnetization on the applied magnetic field and provided an important parameter, the saturation magnetization (M_s) reflecting a concentration of ferrimagnetic component in the particles (Fig. 3a). The nanoparticles exhibited a superparamagnetic behavior, which is important for biomedical applications, as it ensures dispersibility of the particles in an aqueous medium in the absence of magnetic field (M_s = 0), however, the nanoparticles are magnetized and attracted by a magnet.

Superparamagnetic character of the particles was also confirmed the Day diagram [52] illustrating the saturation remanent magnetization M_{rs}/saturation magnetization M_s versus the coercivity of remanence H_{cr}/H_c coercivity ratios (Fig. 3b). The shape of a hysteresis loop was

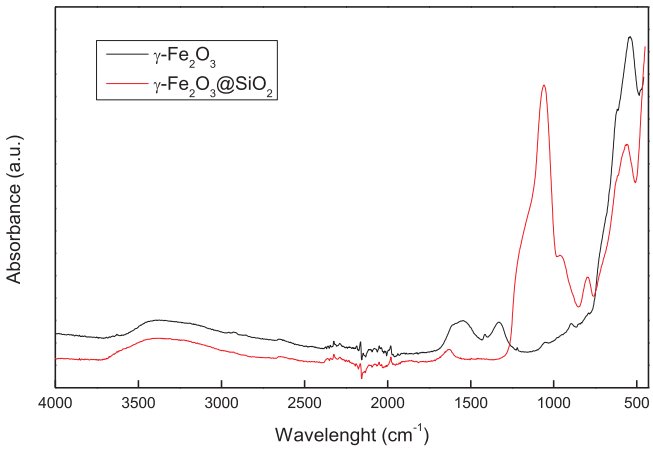

Fig. 2. FTIR spectra of γ-Fe_2O_3 and γ-Fe_2O_3@SiO_2 nanoparticles.

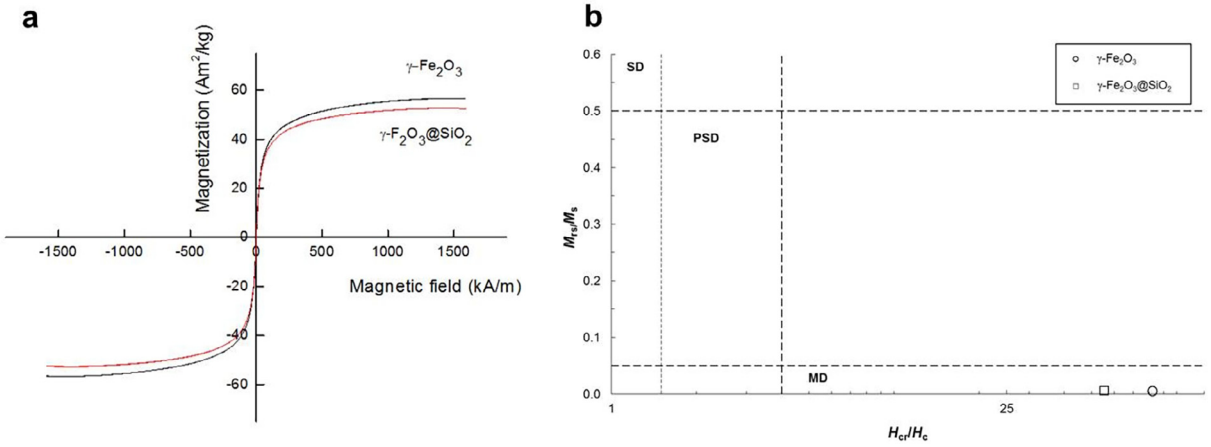

Fig. 3. (a) Hysteresis loops and (b) Day diagram of γ-Fe_2O_3 and γ-Fe_2O_3@SiO_2 nanoparticles. SD, PSD, and MD is single, pseudosingle, and multidomain, respectively.

determined partially by the domain state. There are three types of particle behavior, single domain (SD), multidomain (MD), and pseudo-single domain (PSD) [53]. SD magnetic particles are smallest and have a near-uniform magnetization with all their atomic magnetic moments aligned parallel to each other. When the particles are larger, the magnetic structure breaks into separate regions disconnected by magnetic domain walls (MD). Smaller MD particles, which display SD-like magnetic behavior and have non-uniform magnetizations, are denoted as PSD [54]. Estimation between SD, PSD, and MD behavior depends on many factors, such as particle shape, intensity of the field used to induce the remanence, temperature, etc. When particle size continues to decrease within the SD range (high coercivities and remanence) and the remanence, as well as the coercivity, reach zero, the particle becomes superparamagnetic [55].

It should be noted that the magnetic behavior of the γ-Fe_2O_3 and γ-Fe_2O_3@SiO_2 nanoparticles was different from the bulk maghemite due to the very small size, inter-particle interactions, and surface effects. The saturation magnetization of uncoated γ-Fe_2O_3 particles, determined from the hysteresis loop after subtraction of the linear part, was 56.5 A·m^2/kg suggesting that the concentration of maghemite in the sample was 70.6 wt%, assuming that the saturation magnetization of pure maghemite is 80 A·m^2/kg [56]. After the modification with SiO_2, the magnetization of γ-Fe_2O_3@ SiO_2 particles decreased to 51 A·m^2/kg (Table 1), which corresponds to 63.8 wt% γ-Fe_2O_3 in the composite. This value was approximately in agreement with data determined by AAS (41.5 wt% Fe, i.e., 59.3 wt% γ-Fe_2O_3).

3.3. Treatment of tumor-bearing animals with the particles and/or a vitamin E derivative

As shown in our previous report, poly(*N,N*-dimethylacrylamide-*co*-acrylic acid)-coated γ-Fe_2O_3 induced lipid, protein, and glutathione oxidation *in vitro* in the blood serum, which resulted in profound antitumor activity in mice with Lung Lewis carcinoma [57]. Experiments on the same breed of rats with Walker-256 carcinosarcoma as used in this study then demonstrated that combined administration of γ-Fe_2O_3 with Toc-6-Ac substantially enhanced the antitumor activity compared to treatment with single agents [41]. Antitumor activity of the iron oxide nanoparticles was ascribed to Fe^{2+} release, which increased after addition of Toc-6-Ac [41].

In this report, we investigated antitumor activity of the γ-Fe_2O_3@ SiO_2 nanoparticles on experimental mammary gland carcinosarcoma, assuming that the inert silica shell will reduce the effect. To verify tumor inhibitory effect of Toc-6-Ac, it was administered *per os* both alone and jointly with the γ-Fe_2O_3 or γ-Fe_2O_3@SiO_2 nanoparticles in Wistar rats with W-256 (Fig. 4).

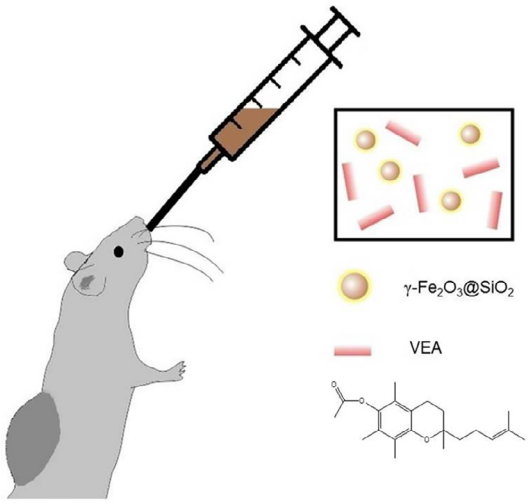

Fig. 4. Schematic illustration of *per os* administration of γ-Fe_2O_3@SiO_2 and Toc-6-Ac in a rat with experimental mammary gland carcinosarcoma. VEA – vitamin E analogue.

Table 2
Combined antitumor effect of vitamin E analogue (Toc-6-Ac) and iron oxide nanoparticles administered *per os* in Wistar rats with Walker-256 mammary gland carcinosarcoma compared to tumor-bearing rats intraperitoneally treated with doxorubicin.

Run	Active substance	Drug or particle dose (mg/kg)	Tumor volume reduction (vol.%)	No. & (%) of animals with complete tumor regression
1	Doxorubicin	1.5	68.11 ± 7.72*	1 (10)
2	Toc-6-Ac	25	68.68 ± 2.44*	1 (10)
3	γ-Fe_2O_3	10	25.10 ± 3.88*	1 (10)
4	γ-Fe_2O_3@SiO_2	10	12.03 ± 3.82	0 (0)
5	γ-Fe_2O_3@PDMA[a]	10	61.89 ± 5.09*	0 (0)
6	γ-Fe_2O_3 + Toc-6-Ac	10 and 25	36.25 ± 2.92*,#	4 (40)
7	γ-Fe_2O_3@SiO_2 + Toc-6-Ac	10 and 25	57.88 ± 10.47*,§	2 (20)
8	γ-Fe_2O_3@PDMA + Toc-6-Ac[a]	10 and 25	63.80 ± 3.56*	0 (0)

*,#,§Significantly different from control tumor-bearing animals without treatment and animals treated with nanoparticles No. 3 and 4, respectively.
[a] From [41]. The data are means ± SE (number of animals n = 10).

Antitumor effect of Toc-6-Ac and iron oxide nanoparticles was compared not only to that of doxorubicin, which was intraperitoneally injected in tumor-bearing rats, but also to γ-Fe_2O_3@PDMA (Table 2).

Tumor inhibitory activity was expressed in terms of tumor volume reduction. Doxorubicin, Toc-6-Ac, and γ-Fe_2O_3 reduced the tumor volume by 68, 69, and 25 vol%, respectively. In contrast, administration of γ-Fe_2O_3@SiO_2 nanoparticles decreased the tumor volume by only ~12 vol% due to the presence of inert SiO_2 shell hindering the redox activity of γ-Fe_2O_3. When Toc-6-Ac was administered in tumor-bearing animals together with γ-Fe_2O_3, moderate tumor volume reduction was noted compared to administration of neat γ-Fe_2O_3 (Table 2). However, if Toc-6-Ac was jointly administered with the γ-Fe_2O_3@SiO_2 nanoparticles, tumor inhibition was boosted reducing the tumor volume by 58 vol%. It can be thus supposed that while the γ-Fe_2O_3 redox activity in the γ-Fe_2O_3@SiO_2 nanoparticles was suppressed, addition of Toc-6-Ac boosted reduction of Fe^{3+} to Fe^{2+} ions even in the presence of the silica shell. Antitumor effect of γ-Fe_2O_3@SiO_2 nanoparticles was lower than that of γ-Fe_2O_3@PDMA nanoparticles (Table 2), which can be explained by very rapid engulfment of γ-Fe_2O_3@PDMA nanoparticles by the cells [43].

Antitumor effect of γ-Fe_2O_3@SiO_2 nanoparticles and Toc-6-Ac on Walker-256 mammary gland carcinosarcoma in Wistar rats was exemplified on Fig. 5.

Tumor even completely disappeared (was undetectable) in some animals treated with the iron oxide nanoparticles and/or Toc-6-Ac (Table 2). Number of animals with complete tumor regression was higher after combined treatment with Toc-6-Ac and γ-Fe_2O_3 or γ-Fe_2O_3@SiO_2 nanoparticles than that treated with doxorubicin, neat γ-Fe_2O_3, Toc-6-Ac, or γ-Fe_2O_3@SiO_2 nanoparticles. Complete tumor regression can be ascribed to Fe^{2+} release from the particles, which was boosted by Toc-6-Ac [41]. When considering the antitumor action of the particles, they are supposed to move from the stomach in the small intestine, from which they can resorb in the blood stream by a mechanism based on absorption of the particles by intestinal villus [58]. Being once in the bloodstream, more particles are absorbed by the highly proliferating tumor cells than by the healthy ones. Moreover, well-known differences between endocytosis pathways of the tumor and healthy cells should be considered [59].

3.4. Cytotoxicity of the nanoparticles on blood cells and liver

To test biological effects of the nanoparticles before and after addition of Toc-6-Ac on Wistar rats with W-256 carcinosarcoma, white and red blood cells were counted in the rat's whole blood (Fig. 6). Number of white blood cells decreased in all groups of the treated tumor-bearing animals compared to the control untreated rats (Fig. 6a). This decrease was dramatic in the animals treated with the γ-Fe_2O_3@SiO_2 nanoparticles; however, number of white blood cells was normalized to that in healthy rats after co-administration with Toc-6-Ac. Reduced number of white blood cells in rats treated with the γ-Fe_2O_3@SiO_2 nanoparticles suggested that the immune system was weak increasing the risk of infection. The normalization of white blood cells counts by co-administration of Toc-6-Ac can be attributed to the stimulation of the immune system. In contrast to white blood cell decrease, no statistically significant changes were observed in red blood cell counts in all groups of the tested animals (Fig. 6b). The absence of changes in red blood cell counts reflects the normal number of erythrocytes containing hemoglobin, which carries oxygen to body's tissues and organs. The low hemoglobin level may result in anemia. The higher red blood cell counts than normal (so-called erythrocytosis) may occur due to abnormalities in the bone marrow.

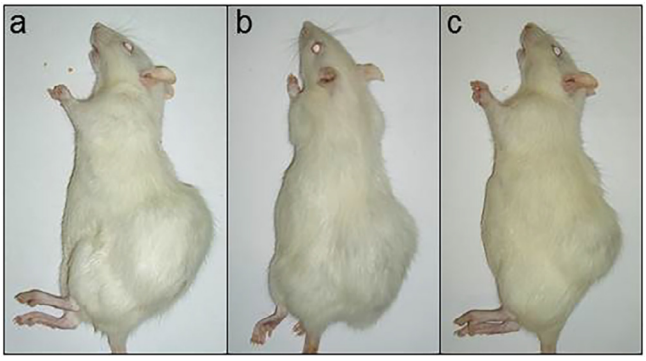

Fig. 5. Antitumor effect of nanoparticles on Walker-256 mammary gland carcinosarcoma (Wistar rats). (a) Untreated rat with tumor (control), (b) rat with tumor treated *per os* by γ-Fe_2O_3@SiO_2 nanoparticles, and (c) γ-Fe_2O_3@SiO_2 + Toc-6-Ac.

In addition to the blood cell tests, the hepatic function of the investigated animals was assessed by measuring ALT and AST activities and bilirubin content in blood plasma (Fig. 7). In all the animal groups, with the exception of tumor-bearing rats treated with γ-Fe_2O_3@SiO_2, both enzyme activities decreased compared to those in untreated animals with W-256 carcinosarcoma (Fig. 7a and b).

This decrease corresponded to that achieved in the rats treated with doxorubicin, which is commonly used an anticancer drug in clinics. In contrast, the ALT and AST results confirmed that the γ-Fe_2O_3@SiO_2 did not change enzyme activity. Compared to both tumor-bearing and intact control rats, bilirubin content decreased in all groups of treated animals, with this decrease being more pronounced in rats treated with γ-Fe_2O_3 and γ-Fe_2O_3@SiO_2 nanoparticles (Fig. 7c). Co-administration of the γ-Fe_2O_3 and γ-Fe_2O_3@SiO_2 particles with Toc-6-Ac normalized bilirubin levels to those of the intact controls. These results thus proved that combined oral administration of γ-Fe_2O_3@SiO_2 nanoparticles with Toc-6-Ac did not induce toxicity in the liver, which is a dominant organ of nanoparticle accumulation [60].

4. Conclusions

Superparamagnetic iron oxide nanoparticles were obtained by a co-precipitation method and coated with silica. We preferred maghemite to magnetite particles since Fe^{2+} ions are known to have higher adverse effects on the cell microenvironment than the Fe^{3+} ions [61,62]. Resulting γ-Fe_2O_3@SiO_2 nanoparticles represent an important example of core-shell particles. While the core provides magnetic property enabling easy and rapid manipulation of the particles in the magnetic field or imaging by MRI, the silica shell renders the particles with biocompatibility and colloidal stability in biological applications. Additional advantage of silica consists in its simple modifiability introducing typically amino or carboxyl groups, that are available for future attachment of target biomolecules.

It can be hypothesized that redox activity of the iron oxide particles is playing a key role in influencing their biological functions [41]. For example, γ-Fe_2O_3@PDMA nanoparticles exhibited a strong antitumor activity in Walker-256 carcinosarcoma-bearing rats, i.e., tumor volume was substantially reduced. In the present report, we have confirmed that coating of γ-Fe_2O_3 particles with silica dramatically decreased the antitumor activity. While the neat γ-Fe_2O_3 reduced the tumor volume by 25 vol%, the γ-Fe_2O_3@SiO_2 particles by only 12 vol%. However, co-administration of the γ-Fe_2O_3@SiO_2 particles with Toc-6-Ac substantially boosted the antitumor activity, as documented by reduction of the tumor volume by 58 vol% and complete tumor regression in 20% of animals. This antitumor effect was explained by Fe^{2+} release from γ-Fe_2O_3 particles, which is in agreement with our previous report [41].

This study thus offered a new experimental approach for prospective effective treatment in oncology using a combined oral administration of silica-modified superparamagnetic nanoparticles together with Toc-6-Ac. This joint application lacks undesirable toxic side-effects, which are typical for doxorubicin. The finding can be exploited in the future design of magnetically manipulatable and

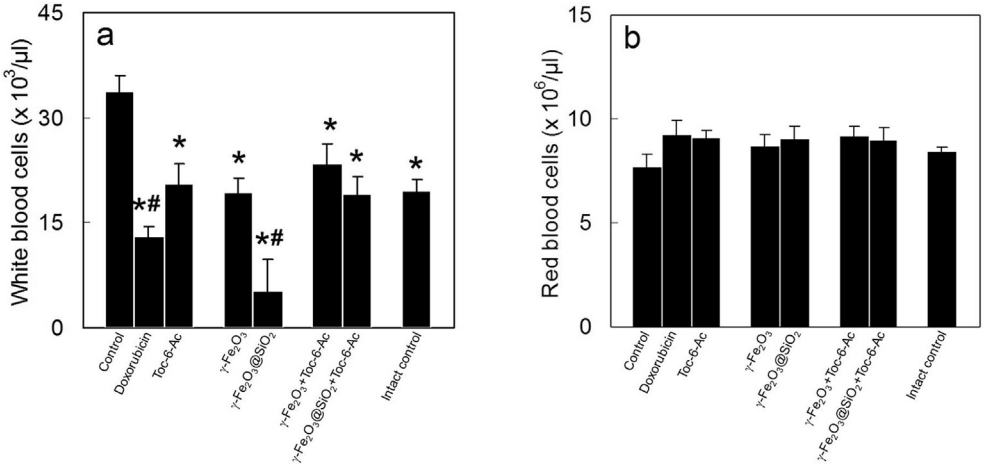

Fig. 6. *In vivo* blood count of (a) white and (b) red blood cells in Walker-256 carcinosarcoma-bearing Wistar rats treated with doxorubicin (1.5 mg), Toc-6-Ac (25 mg), γ-Fe_2O_3 (10 mg), γ-Fe_2O_3@SiO_2 (10 mg), γ-Fe_2O_3 (10 mg) + Toc-6-Ac (25 mg), γ-Fe_2O_3@SiO_2 (10 mg) + Toc-6-Ac (25 mg) per kg of body weight. Control – no treatment of tumor-bearing rats; intact control – non-treated rats without tumor. The data are means ± SE (n = 7–9). $^{*,\ \#}$ are significantly different from control tumor-bearing animals and intact control, respectively.

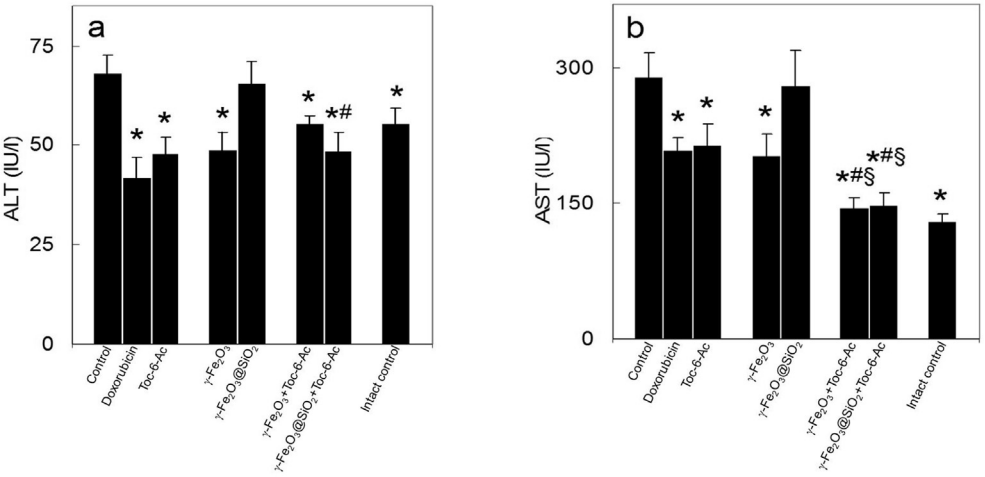

Fig. 7. *In vivo* determination of hepatic function using (a) ALT, (b) AST, and (c) bilirubin analysis in blood plasma of Wistar rats with Walker-256 mammary gland carcinosarcoma treated with doxorubicin (1.5 mg), Toc-6-Ac (25 mg), γ-Fe_2O_3 (10 mg), γ-Fe_2O_3@SiO_2 (10 mg), γ-Fe_2O_3 (10 mg) + Toc-6-Ac (25 mg), γ-Fe_2O_3@SiO_2 (10 mg) + Toc-6-Ac (25 mg) per kg of body weight. Control – no treatment of tumor-bearing rats; intact control – non-treated rats without tumor. ALT – alanine aminotransferase, AST – aspartate aminotransferase. The data are means ± SE (n = 7–9). $^{*,\S,\#}$ are significantly different from control tumor-bearing animals, animals treated with doxorubicin, and γ-Fe_2O_3 and γ-Fe_2O_3@SiO_2, respectively.

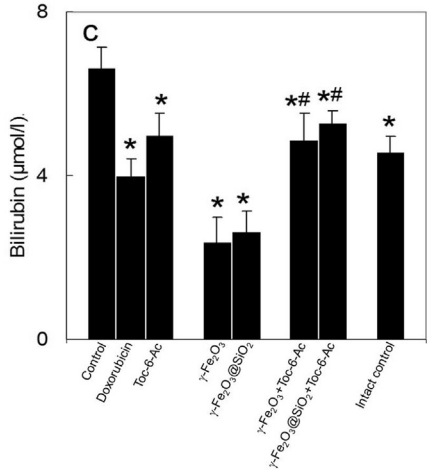

targetable redox-active anticancer agents. However, more studies on polymer-coated iron oxide nanoparticles are required using different experimental tumors than the mammary gland.

Acknowledgment

The financial support of the Czech Science Foundation (grant 17-04918S) and RECOOP HST Association and Cedars-Sinai Medical Center is acknowledged.

Appendix A. Supplementary data

Supplementary data to this article can be found online at https://doi.org/10.1016/j.jmmm.2018.10.006.

References

[1] A.K. Gupta, M. Gupta, Synthesis and surface engineering of iron oxide nanoparticles for biomedical applications, Biomaterials 26 (2005) 3995–4021.
[2] W. Wu, Z.H. Wu, T. Yu, C.Z. Jiang, W.S. Kim, Recent progress on magnetic iron oxide nanoparticles: synthesis, surface functional strategies and biomedical

applications, Sci. Technol. Adv. Mater. 16 (2015) 023501.
[3] A. Orza, H. Wu, Y. Xu, Q. Lu, H. Mao, One-step facile synthesis of highly magnetic and surface functionalized iron oxide nanorods for biomarker-targeted applications, ACS Appl. Mater. Interfaces 9 (2017) 20719–20727.
[4] J. Mosayebi, M. Kiyasatfar, S. Laurent, Synthesis, functionalization, and design of magnetic nanoparticles for theranostic applications, Adv. Healthcare Mater. 6 (2017) 1700306.
[5] N. Lee, T. Hyeon, Designed synthesis of uniformly sized iron oxide nanoparticles for efficient magnetic resonance imaging contrast agents, Chem. Soc. Rev. 41 (2012) 2575–2589.
[6] D. Smejkalová, K. Nešporová, G. Huerta-Angeles, J. Syrovátka, D. Jirák, A. Gálisová, V. Velebný, Selective *in vitro* anticancer effect of superparamagnetic iron oxide nanoparticles loaded in hyaluronan polymeric micelles, Biomacromolecules 10 (2014) 4012–4020.
[7] J. Gallo, N.J. Long, E.O. Aboagye, Magnetic nanoparticles as contrast agents in the diagnosis and treatment of cancer, Chem. Soc. Rev. 42 (2013) 7816–7833.
[8] J.P. Fortin, C. Wilhelm, J. Servais, C. Ménager, J.C. Bacri, F. Gazeau, Size-sorted anionic iron oxide nanomagnets as colloidal mediators for magnetic hyperthermia, J. Am. Chem. Soc. 129 (2007) 2628–2635.
[9] R. Hergt, S. Dutz, R. Müller, M. Zeisberger, Magnetic particle hyperthermia: nanoparticle magnetism and materials development for cancer therapy, J. Phys.: Condens. Matter 18 (2006) 2919–2934.
[10] N. Sangeetha, A.K. Kumaraguru, Antitumor effect and characterization of biosythesized iron oxide nanoparticles using sea weeds of gulf of mannar, Int. J. Pharm. Pharm. Sci. 7 (2015) 469–476.
[11] T.K. Jain, M.A. Morales, S.K. Sahoo, D.L. Leslie-Pelecky, V. Labhasetwar, Iron oxide nanoparticles for sustained delivery of anticancer agents, Mol. Pharm. 2 (2005) 194–205.
[12] J.K. Oh, J.M. Park, Iron oxide-based superparamagnetic polymeric nanomaterials: design, preparation, and biomedical application, Prog. Polym. Sci. 36 (2011) 168–189.
[13] S. Laurent, D. Forge, M. Port, A. Roch, C. Robic, L.V. Elst, R.N. Muller, Magnetic iron oxide nanoparticles: synthesis, stabilization, vectorization, physicochemical characterizations, and biological applications, Chem. Rev. 108 (2008) 2064–2110.
[14] M. Timko, M. Molčan, A. Hashim, A. Skumiel, M. Muller, H. Gojzewski, A. Jozefczak, J. Kovac, M. Rajnak, M. Makowski, P. Kopčanský, Hyperthermic effect in suspension of magnetosomes prepared by various methods, IEEE Trans. Magn. 49 (2013) 250–254.
[15] R. Ladj, A. Bitar, M. Eissa, Y. Mugnier, R. Le Dantec, H. Fessi, A. Elaissari, Individual inorganic nanoparticles: preparation, functionalization and *in vitro* biomedical diagnostic applications, J. Mater. Chem. B 1 (2013) 1381–1396.
[16] A.G. Roca, M.P. Morales, K.O. Grady, C.J. Serna, Structural and magnetic properties of uniform magnetite nanoparticles prepared by high temperature decomposition of organic precursors, Nanotechnology 17 (2006) 2783–2788.
[17] N.S. Farheen, P. Vivek, Facile and sustainable synthesis of shaped iron oxide nanoparticles: effect of iron precursor salts on the shapes of iron oxides, Sci. Rep. 5 (2015) 9733.
[18] S.C. McBain, H.H.P. Yiu, J. Dobson, Magnetic nanoparticles for gene and drug delivery, Int. J. Nanomed. 3 (2008) 169–180.
[19] J.R. McCarthy, R. Weissleder, Multifunctional magnetic nanoparticles for targeted imaging and therapy, Adv. Drug Deliv. Rev. 60 (2008) 1241–1251.
[20] W. Wu, Q. He, J. Changzhong, Magnetic iron oxide nanoparticles: synthesis and surface functionalization strategies, Nanoscale Res. Lett. 3 (2008) 397–415.
[21] R. Ladj, A. Bitar, M. Eissa, H. Fessi, Y. Mugnier, R. Le Dantec, A. Elaissari, Encapsulation of inorganic nanoparticles for biomedical applications, Int. J. Pharm. 458 (2013) 230–241.
[22] P. Yang, J.Y. Zhao, L.Y. Hou, L. Yang, K. Wu, L.Y. Zhang, Vitamin E succinate induces apoptosis via the PI3K/AKT signaling pathways in EC109 esophageal cancer cells, Mol. Med. Rep. 14 (2016) 1531–1537.
[23] R.P. Singh, G. Sharma, Sonali, S. Singh, M. Kumar, B.L. Pandey, B. Koch, M.S. Muthu, Vitamin E TPGS conjugated carbon nanotubes improved efficacy of docetaxel with safety for lung cancer treatment, Colloids Surf. B 141 (2016) 429–442.
[24] A. Angulo-Molina, M.A. Mendez-Rojas, T. Palacios-Hernandez, O.E. Contreras-Lopeze, G.A. Hirata-Florese, J.C. Flores, K.L. Flores, C. Velazquez, R. Robles-Zepeda, E. Silva-Campa, A. Sarabia, M. Barboza-Flores, M. Pedroza-Montero, J.R. Reyes-Leyva, J. Hernandez, Magnetite nanoparticles functionalized with vitamin E analogues: anticancer effects, Mater. Today-Proc. 3 (2016) 703–707.
[25] C. Constantinou, A. Papas, A.I. Constantinou, Vitamin E and cancer: an insight into the anticancer activities of vitamin E isomers and analogs, Int. J. Cancer 123 (2008) 739–752.
[26] J. Yang, L. Wang, Z.L. Chen, Z.Q. Shen, M. Jin, X.W. Wang, Y.F. Zheng, Z.G. Qiu, J.F. Wang, J.W. Li, Antioxidant intervention of smoking-induced lung tumor in mice by vitamin E and quercetin, BMC Cancer 8 (2008) 383.
[27] C. Yang, T. Wu, Y. Qi, Z. Zhang, Recent advances in the application of vitamin E TPGS for drug delivery, Theranostics 8 (2018) 464–485.
[28] S. Tan, C. Zou, W. Zhang, M. Yin, X. Gao, Q. Tang, Recent developments in d-α-tocopheryl polyethylene glycol-succinate-based nanomedicine for cancer therapy, Drug. Deliv. 24 (2017) 1831–1842.
[29] J. Neuzil, Vitamin E succinate and cancer treatment: a vitamin E prototype for selective antitumour activity, Br. J. Cancer 89 (2003) 1822–1826.
[30] Z. Zhang, S. Tan, S.S. Feng, Vitamin E TPGS as a molecular biomaterial for drug delivery, Biomaterials 33 (2012) 4889–4906.
[31] Z. Zhang, L. Mei, S.-S. Feng, Vitamin E D-α-tocopheryl polyethylene glycol 1000 succinate-based nanomedicine, Nanomedicine 7 (2012) 1645–1647.
[32] M.P. Malafa, L.T. Neitzel, Vitamin E succinate promotes breast cancer tumor dormancy, J. Surg. Res. 93 (2000) 163–170.
[33] X.-F. Wang, L. Dong, Y. Zhao, M. Tomasetti, K. Wu, J. Neuzil, Vitamin E analogues as anticancer agents: lessons from studies with α-tocopheryl succinate, Mol. Nutr. Food Res. 50 (2006) 675–685.
[34] A. Bitar, N.M. Ahmad, H. Fessi, A. Elaissari, Silica based nanoparticles for biomedical applications, Drug Discov. Today 17 (2012) 1147–1154.
[35] K.A. Lawson, K. Anderson, M. Menchaca, J. Atkinson, L. Sun, V. Knight, B.E. Gilbert, C. Conti, B.G. Sanders, K. Kline, Novel vitamin E analogue decreases syngeneic mouse mammary tumor burden and reduces lung metastasis, Mol. Cancer Ther. 2 (2003) 437–444.
[36] C.M. Sims, S.K. Hanna, D.A. Heller, C.P. Horoszko, M.E. Johnson, A.R. Montoro Bustos, V. Reipa, K.R. Riley, B.C. Nelson, Redox-active nanomaterials for nanomedicine applications, Nanoscale 9 (2017) 15226–15251.
[37] A. Rahman, Y. Matsumura, S. Yano, B. Ochiai, pH-Responsive charge-conversional and hemolytic activities of magnetic nanocomposite particles for cell-targeted hyperthermia, ACS Omega 3 (2018) 961–972.
[38] J. Chomoucka, J. Drbohlavova, D. Huska, V. Adam, R. Kizek, J. Hubalek, Magnetic nanoparticles and targeted drug delivering, Pharmacol. Res. 62 (2010) 144–149.
[39] F. Ye, J. Qin, M.S. Toprak, M. Muhammed, Multifunctional core-shell nanoparticles: superparamagnetic, mesoporous, and thermosensitive, J. Nanopart. Res. 13 (2011) 6157–6167.
[40] W. Stöber, A. Fink, Controlled growth of monodisperse silica spheres in the micron size range, J. Colloid Interface Sci. 26 (1968) 62–69.
[41] D. Horák, V.I. Pustovyy, A.V. Babinskiy, O.M. Palyvoda, V.F. Chekhun, I.N. Todor, O.I. Kuzmenko, Enhanced antitumor activity of surface-modified iron oxide nanoparticles and α-tocopherol derivative in a rat model of mammary gland carcinosarcoma, Int. J. Nanomed. 12 (2017) 4257–4268.
[42] G.V. Donchenko, Y.D. Kholodova, I.V. Kuzmenko, K.P. Klymenko, Inhibitor of Cancer Growth, (1998) UA Patent, 23977 UA.
[43] B.A. Zasońska, N. Boiko, D. Horák, O. Klyuchivska, H. Macková, M. Beneš, M. Babič, M. Trchová, J. Hromádková, R. Stoika, The use of hydrophilic poly(*N,* N-dimethylacrylamide) grafted from magnetic γ-Fe_2O_3 nanoparticles to promote engulfment by mammalian cells, J. Biomed. Nanotechnol. 9 (2013) 479–491.
[44] B.A. Zasońska, N. Boiko, O. Klyuchivska, M. Trchová, E. Petrovský, R. Stoika, D. Horák, Silica-coated γ-Fe_2O_3 nanoparticles: preparation and engulfment by mammalian macrophages, J. Nanopharm. Drug Deliv. 1 (2013) 182–192.
[45] M.I. Walters, H.W. Gerarde, An ultramicromethod for the determination of conjugated and total bilirubin in serum or plasma, Microchem. J. 15 (1970) 231–243.
[46] K.S. Henley, IFCC method for alanine aminotransferase, Clin. Chim. Acta 105 (1980) 155–166.
[47] H.U. Bergmeyer, M. Horder, D.W. Moss, Provisional recommendations on IFCC methods for the measurements of catalytic concentrations of enzymes. Part 3. Revised IFCC method for aspartate aminotransferase, Clin. Chem. 24 (1978) 720–721.
[48] A. Faustino-Rocha, P.A. Oliveira, J. Pinho-Oliveira, C. Teixeira-Guedes, R. Soares-Maia, R.G. da Costa, B. Colaço, M.J. Pires, J. Colaço, R. Ferreira, M. Ginja, Estimation of rat mammary tumor volume using caliper and ultrasonography measurements, Lab. Anim. 42 (2013) 217–224.
[49] B. Close, K. Banister, V. Baumans, E. Bernoth, N. Bromage, J. Bunyan, W. Erhardt, P. Flecknell, N. Gregory, H. Hackbarth, D. Morton, C. Warwick, Recommendations for euthanasia of experimental animals: Part 1, Lab. Anim. 30 (1996) 293–316.
[50] B. Close, K. Banister, V. Baumans, E. Bernoth, N. Bromage, J. Bunyan, W. Erhardt, P. Flecknell, N. Gregory, H. Hackbarth, D. Morton, C. Warwick, Recommendations for euthanasia of experimental animals: Part 2, Lab. Anim. 31 (1997) 1–32.
[51] C.J. Brinker, G.W. Scherrer, Sol Gel Science, The Physics and Chemistry of Sol-Gel Processing, Academic Press, San Diego, 1990.
[52] R. Day, M. Fuller, V.A. Schmidt, Hysteresis properties of titanomagnetites: grain-size and compositional dependence, Phys. Earth. Planet. Inter. 13 (1977) 260–267.
[53] F.D. Stacey, A generalized theory of thermoremanence, covering the transition from single domain to multi-domain magnetic grains, Philos. Magn. 7 (1962) 1887–1900.
[54] A. Muxworthy, The role of magnetic interactions in natural systems, Astron. Geophys. 2 (31-2) (54 2013,) 35.
[55] G. Schubert, Treatise on Geophysics, Elsevier, Amsterdam, 2015, p. 152.
[56] R.M. Cornell, U. Schwertmann, The Iron Oxides: Structure, Properties, Reactions, Occurrence and Uses, VCH, New York, 1996, p. 117.
[57] H. Macková, D. Horák, V.F. Donchenko, V.I. Andriyaka, O.M. Palyvoda, V.I. Chernishov, V.F. Chekhun, I.N. Todor, O.I. Kuzmenko, Colloidally stable surface-modified iron oxide nanoparticles: preparation, characterization and antitumor activity, J. Magn. Magn. Mater. 380 (2015) 125–131.
[58] A.M. Hillery, A.W. Lloyd, J. Swarbrick, Drug Delivery and Targeting: For Pharmacists and Pharmaceutical Scientists, Taylor & Francis, New York, 2001.
[59] I. Mellman, Y. Yarden, Endocytosis and cancer, Cold Spring Harb. Perspect. Biol. 5 (2013) a016949.
[60] M.F. Hughes, T.C. Long, W.K. Boyes, R. Ramabhadran, Whole-body retention and distribution of orally administered radiolabelled zerovalent iron nanoparticles in mice, Nanotoxicology 7 (2013) 1064–1069.
[61] A.V. Singh, V. Vyas, E. Maontani, D. Cartelli, D. Parazzoli, A. Oldani, G. Zeri, E. Orioli, D. Gemmati, P. Zamboni, Investigation of *in vitro* cytotoxicity of the redox state of ionic iron in neuroblastoma cells, J. Neurosci. Rural Pract. 3 (2012) 301–310.
[62] M. Karami, M.A. Ebrahimzadeh, M.R. Mahdavi, A. Kazemi, Effect of Fe^{2+} and Fe^{3+} ions on human plasma cholinesterase activity, Eur. Rev. Med. Pharmacol. Sci. 14 (2010) 897–901.